ADVANCED
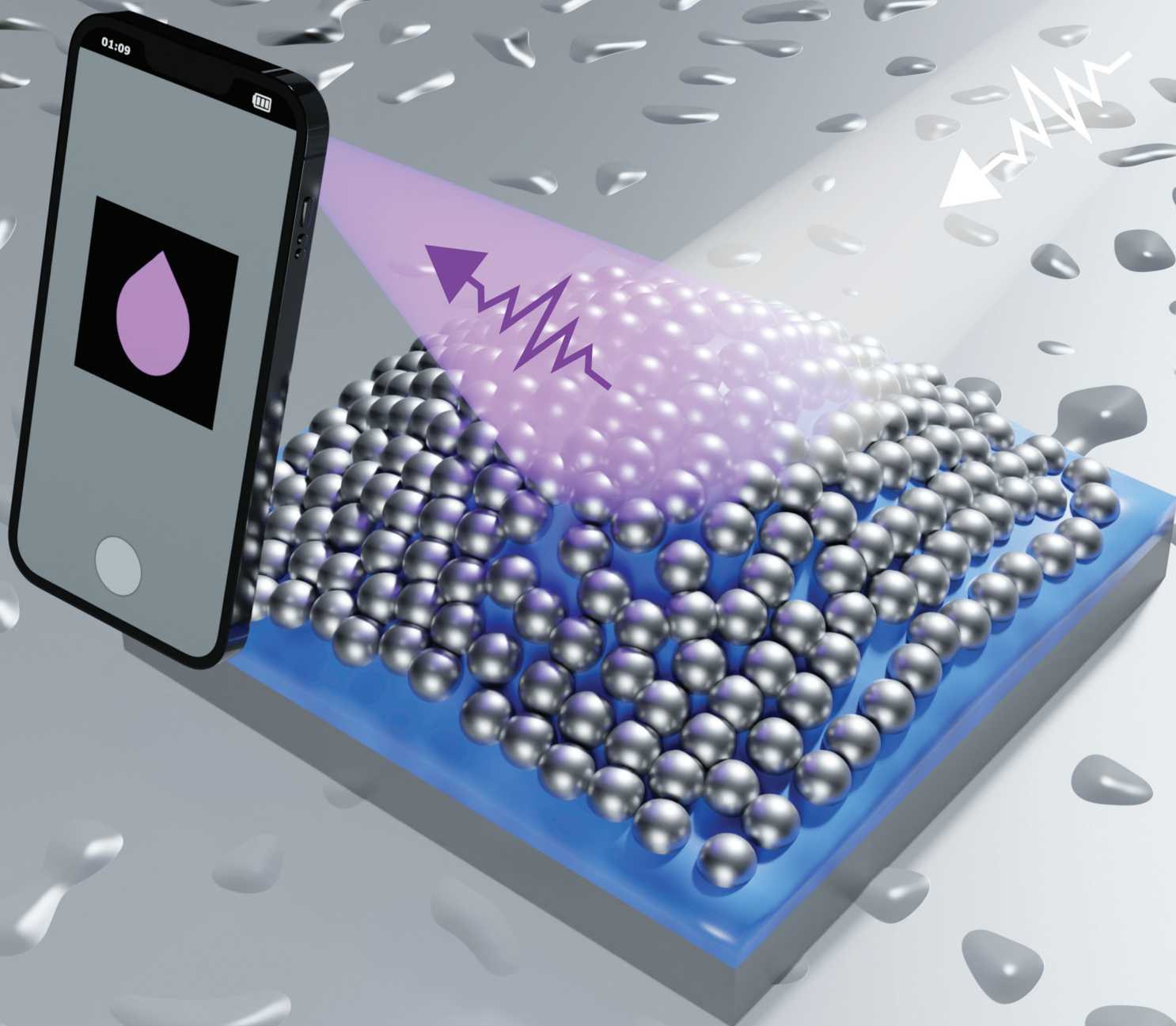## OPTICAL
MATERIALS

Reusable Structural Colored Nanostructure for Powerless Temperature and Humidity Sensing

*Pablo Cencillo-Abad, Pamela Mastranzo-Ortega, Divambal Appavoo, Tianyi Guo, Lei Zhai, Javier Sanchez-Mondragon, and Debashis Chanda**

Nanostructured materials have enabled new ways of controlling the light–matter interaction, opening new routes for exciting applications, in display technologies and colorimetric sensing, among others. In particular, metallic nanoparticles permit the production of color structures out of colorless materials. These plasmonic structural colors are sensitive to the environment and thus offer an interesting platform for sensing. Here, a self-assembly of aluminum nanoparticles in close proximity of a mirror is spaced by an ultrathin poly(N-isopropylacrylamide) (PNIPAM) layer. Hybridizing the plasmonic system with the active polymer layer, a thermoresponsive gap-plasmon architecture is formed that transduces changes in the temperature and relative humidity of the environment into color changes. By harnessing the environmentally induced structural changes of PNIPAM, it was estimated from the finite difference time domain simulation that the resonance can be tuned 7 nm per every 1 nm change in thickness, resulting in color variation. Importantly, these fully reversible changes can be used for reusable powerless humidity and temperature colorimetric sensing. Crucially if condensation on the structure happens, the polymer layer is deformed beyond recovery and the colors are washed away. We leverage this effect to produce tamper-proof dew labels that a straightforward smartphone app can read by taking a picture.

1. Introduction

Nanotexturing of materials enables new ways of controlling the light–matter interaction. At the nanoscale, in contrast to bulk materials, material's properties show a strong dependence on size and shape. When electromagnetic waves interact with a metallic nanoparticle, light can drive the free electrons of the conduction band in a collective oscillation, named localized plasmons, leading to strong optical absorption.[1,2] Crucially, this resonant response shows a marked dependence on the composition, size, spatial arrangement, and environment of the structure.[1,3] In a manner, nanoparticles act as optical antennas that confine the light at deep-subwavelength volumes producing extraordinary enhancement of the near field.[4] Plasmonic resonances can thus be exploited to control the spectral and spatial response of materials to impinging light, opening new routes for exciting applications, among others, in holography, wave front engineering, display technologies, sensing, or structural coloration.[5–9] The production of artificial structural colors by exploiting plasmonic resonances has gained great attention in recent years.[10–13] In plasmonic coloration, the color is the result of the absorption of specific bands of the incoming light by the constituent metallic nanoparticles. Importantly, these absorption bands can be readily tuned by changing the geometric parameters of the structure or the material properties, thus tuning the color appearance. Hence, if a plasmonic structure experiences an external stimulus that changes the material properties, its geometry, or the environmental conditions, the color appearance will change. In other

P. Cencillo-Abad, P. Mastranzo-Ortega, D. Appavoo, T. Guo, L. Zhai, D. Chanda
NanoScience Technology Center
University of Central Florida
12424 Research Parkway Suite 400, Orlando, FL 32826, USA
E-mail: debashis.chanda@ucf.edu
P. Mastranzo-Ortega, J. Sanchez-Mondragon
National Institute of Astrophysics
Optics
and Electronics (INAOE)
Luis Enrique Erron. 1, Sta. María Tonanzintla, Puebla 72840, Mexico

L. Zhai
Department of Chemistry
University of Central Florida
4111 Libra Drive, Orlando, FL 32826, USA
L. Zhai
Department of Materials Science and Engineering
University of Central Florida
12760 Pegasus Drive, Orlando, FL 32826, USA
D. Chanda
Department of Physics
University of Central Florida
4111 Libra Drive, Physical Sciences Bldg. 430, Orlando, FL 32816, USA
D. Chanda
CREOL
The College of Optics and Photonics
University of Central Florida
4304 Scorpius St., Orlando, FL 32816, USA

**ADVANCED
SCIENCE NEWS**

www.advancedsciencenews.com

**ADVANCED
OPTICAL
MATERIALS**

www.advopticalmat.de

words, nanostructures can transduce changes in the structure or environment into changes of the optical response, thus offering a convenient platform for sensing.[14–20]

Many polymers offer structural and material tunability with external stimuli such as electric fields, mechanical stress, temperature, humidity, or environmental pH.[21–23] Introducing these responsive polymers in a structural coloration architecture offers a native and simple route to colorimetric sensing with chemical and biomedical applications.[24] An active polymer that has gained attention in recent years is poly(N-isopropylacrylamide) (PNIPAM).[25–29] PNIPAM is a thermoresponsive polymer that exhibits a sharp lower critical solution temperature (LCST) transition from a hydrophobic to a hydrophilic phase at about 32 °C. This reversible phase transition is the result of hydrogen bonding changes in the polymer chains.[30,31] While at temperatures below LCST the polymer absorbs water and swells, when the temperature is raised above the LCST, the polymer transits to a hydrophobic state that expels absorbed water and decreases its volume. Typically, for temperature sensing applications, a layer of PNIPAM is deposited on top of an already existing plasmonic structure. When the temperature is varied, the polymer undergoes a phase transition that results in a conformal change of the polymer layer, thus altering the metallic resonators' environment and resulting in noticeable changes of the sensor's optical response.[32] In this manner, these hybrid structures work as refractive index sensors. However, most of these approaches rely on grafting PNIPAM brushes on top of the plasmonic substrate.[33–37] While this offers a readily application, large-scale production of such sensors is limited by the time and difficulty of the process, the required environmental conditions during the growth, the limited densities of brushes, and the substrates' compatibility.[38,39] Recently, spun coated ultrathin PNIPAM films have been studied as an alternative.[40–43] Interestingly, these ultrathin films present substantial changes when compared to their brush counterparts. Particularly, for these films, the increased surface/volume ratio makes interface contributions critical and permits the absorption of water from air.[44] In other words, the transition of ultrathin films of PNIPAM is not only dependent on temperature, but also on the amount of water of the surrounding environment.[45] Hence, sensors based on ultrathin PNIPAM can be integrated with plasmonic structures for both temperature and humidity detection.

Here, we present a hybrid PNIPAM/plasmonic nanostructure that changes color appearance in response to thermal or humidity changes in the environment. Gap-plasmon modes can be excited by growing a metallic self-assembled layer of aluminum nanoparticles in close proximity of a back mirror. These optical modes, which result in strong optical absorption at specific visible bands, subtract from incoming light specific wavelengths and thus produce color. The spectral position of the resonance can be tuned by small changes in the geometrical parameters of the structure, namely, the self-assembly or the spacing layer thicknesses, to tune the color appearance. By choosing an ultrathin PNIPAM layer as the spacer between the self-assembly and the back mirror, the spectral position of the resonant mode can thus be tuned with temperature and environmental humidity. In this work, we study how both stimuli induce changes in the PNIPAM layer that results in color variations of the structure. In particular, at the hydrophilic phase (temperatures below LCST), we esti-

mate a spectral shift of 7 nm corresponding to every 1 nm change in PNIPAM thickness, thus offering an interesting opportunity for powerless and reusable nanosensors for temperature and humidity colorimetric monitoring. Furthermore, when condensation happens at temperatures below LCST, the PNIPAM losses its conformability and color is washed irreversibly. We propose that, exploiting this irreversibility after condensation, the hybrid nanosensors can thus be used as tamper-proof dew labels. We develop a simple code that analyzes a picture taken with a phone camera to determine the validity of the sensor producing very robust results. Importantly, as these films are simply transferred by spin coating into the target substrate, and conventional evaporation techniques are used for the aluminum self-assembly, their integration in industrial setting is secured, thus highlighting the practicality of the approach.

2. Results

2.1. Hybrid PNIPAM/Plasmonic Sensor

The proposed hybrid polymer/plasmonic sensor consists of a layer of highly packed self-assembled aluminum nanoparticles grown on top of an ultrathin layer of PNIPAM polymer deposited over an aluminum backplane as shown in **Figure 1**a. The stack is sequentially built by evaporating over a substrate an optically thick layer of aluminum. On top of this layer, PNIPAM is spun coated to achieve a thin active spacer. Finally, a self-assembly of aluminum nanoparticles is evaporated on top of the stack by an ebeam evaporator operated at low rate. Further details of the fabrication process and material parameters of the samples used in this study are given in the Experimental Section. Details on the growth dynamics of the self-assembly exceed the scope of this paper and can be found in our earlier publications.[46,47]

Under ambient illumination, the free electrons of the nanoparticles' metal can be coupled to the external light, collectively oscillating in what is termed a localized surface plasmon. While at wavelengths matching the plasmon resonance light is strongly absorbed, off-resonance components are back reflected by the aluminum mirror producing vivid colors. Crucially, as the plasmonic self-assembly is in close proximity to the back mirror, the electromagnetic mode is coupled to the ultrathin cavity and is thus extremely sensitive to changes in the stack geometry while remaining relatively angle and polarization independent. In this manner, the structures produce color by subtracting from white impinging light the bands corresponding to the plasmon resonances. Hence, if the resonance condition varies as a result of a change in the structure, either the nanoparticles sizes or the spacer thickness, the color will change. As stated before, PNIPAM is a thermoresponsive polymer that exhibits a sharp LCST around 32 °C. Above this temperature, the polymer transits to a hydrophobic state where water bonded to the polymer chains is expelled, and the thickness of the layer reduces. As a result of this reduction in volume of the PNIPAM layer, the overall cavity will be affected, and the resonance wavelength for the gap-plasmon will be tuned to shorter wavelengths, with a consequent increase in the red components of the reflected light. On the other hand, as the temperature of the stack is lowered below LCST, the polymer transits to a hydrophilic phase where water is absorbed by the polymer layer, resulting in an increase of the
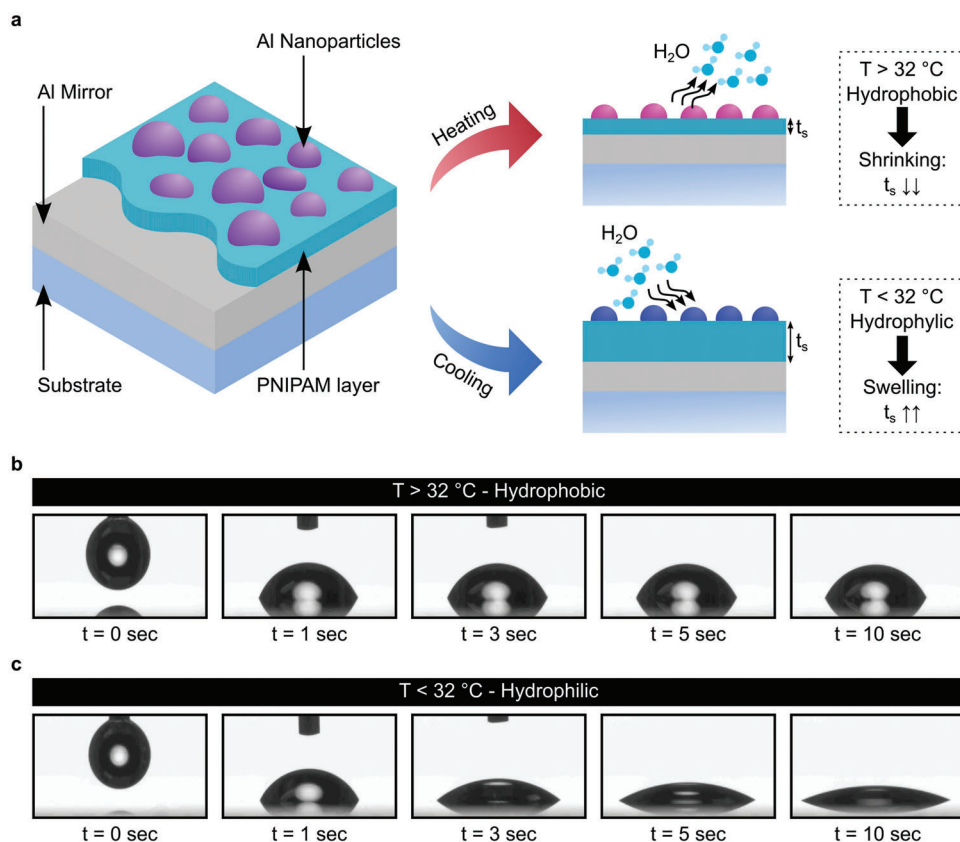
ADVANCED
SCIENCE NEWS
www.advancedsciencenews.com

ADVANCED
OPTICAL
MATERIALS
www.advopticalmat.de

Figure 1. a) The active color nanostructure consists of an aluminum self-assembled layer on top of an ultrathin PNIPAM film over a back mirror. The metallic particles sustain gap-plasmon resonances that can be tuned with the thickness of the spacer. When the temperature is below LCST, the PNIPAM absorbs water and swells, above the LCST, the PNIPAM expels the absorbed water and shrinks. b) At temperatures above the LCST, PNIPAM is hydrophobic, and water cannot bond to the polymer layer. c) If the temperature of the sensor is lowered below LCST, the PNIPAM transitions to a hydrophilic phase and water is again absorbed.

thickness, and a subsequent red-shift of the resonant wavelength that manifests in more blue components on the reflected light, Figure 1a-right.

The change in the phase for the polymer can be further assessed from contact angle measurements. We suspend a 10 µL droplet of water on the nanosensor at temperatures above and below the LCST and monitor the dynamic behavior. As expected, at a temperature of 50 °C, corresponding to a temperature above the LCST, we observe how the droplet remains in the surface for long time with no apparent change in the contact angle, as can be seen in Figure 1b. This behavior corresponds to the hydrophobic phase of the PNIPAM polymer. In contrast, if the sensor is kept at a temperature lower than the LCST, about 20 °C, we observe how the contact angle decreases dynamically with time as the water is absorbed by the polymer, corresponding to the hydrophilic phase, Figure 1c. Furthermore, we note that once the water comes into contact with the sensor at lower temperatures, the color vanishes completely. In contrast to previously reported experiments with grafted PNIPAM, the thin film cannot recover from this saturation, and the structure gets deformed permanently. This nonreversible behavior will be later discussed for its potential in application as tamper-resistant condensation labels. Videos corresponding to the contact-angle experiment in Figure 1b,c, can be found in the Supporting Information.

2.2. Thermal and Humidity Tunable Optical Response based on Gap-Plasmon Dispersion

PNIPAM ultrathin films have been reported to change in response to both temperature and humidity changes in the environment. Hence, both stimuli are expected to change the color of the structure. To analyze both contributions, we use a custom-made sealed gas chamber where nitrogen/water vapor can be injected to reduce/increase the relative humidity (RH). The chamber is placed over a thermostage that controls the temperature of the sensor. Furthermore, the chamber is equipped with an optically transparent window to perform real-time spectroscopy measurements. Thus, by fixing either the temperature or the RH and varying the other parameter, we can decouple both contributions. We first explore the effect of temperature at a constant amount of water in atmosphere by sealing a sensor consisting of 5 nm thickness mass equivalent aluminum nanoparticles, and 35.5 nm PNIPAM polymer at room temperature (20 °C) with RH of 50%. With the environment sealed, we heat and cool the sample to 10 and 40 °C and observe the color change of the structure (**Figure 2**a). An apparent color change is obvious from the sample photography. When cooling down, the sensor absorbs water from the environment and swells, and produces a red-shift on the absorption of the plasmonic system, thus reducing some
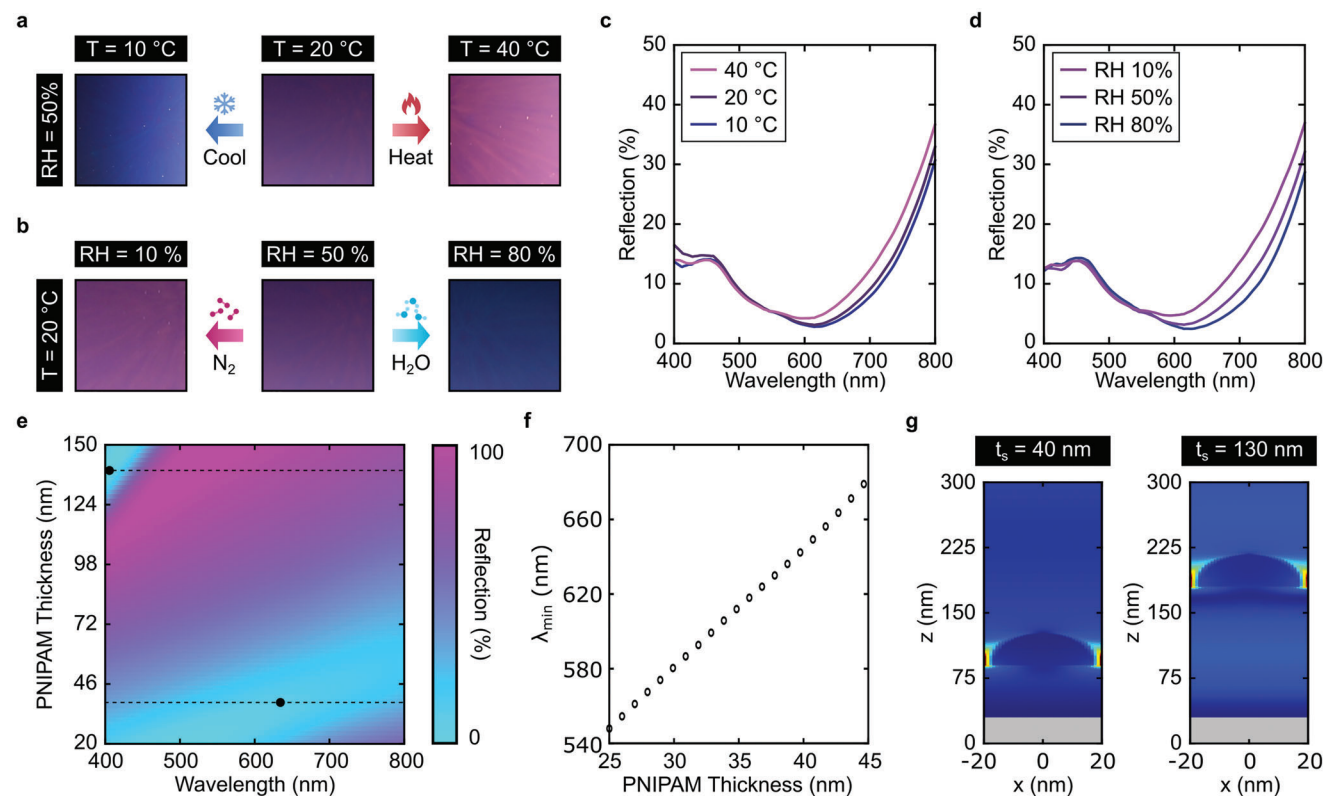
Figure 2. a) By heating/cooling the structure above/below LCST, the PNIPAM layer transitions to the hydrophobic/hydrophilic phase and absorbs/expels the water changing its volume and resulting in color change. b) Changes in the volume of the PNIPAM can also be produced by changing the water content of the environment. To maintain chemical equilibrium, water is released by the PNIPAM in dry atmospheres, whereas water will be absorbed if the atmosphere becomes saturated. c,d) Reflection curves for samples in (a) and (b), respectively. e) FDTD simulation of the reflection curves for different thicknesses of PNIPAM. The resonance red-shifts with the higher thickness, resulting in bluer hues. f) Dependence of the spectral position of the reflection minima with respect to the thickness as obtained in (e). g) Electric field enhancement of the nanoparticle for both thicknesses.

red components in the reflected light. On the contrary, when the sensor is heated, water is expelled by the system and the sensor shrinks, reducing the cavity length and increasing the red components of the reflected wave. It should be noted that, as in any subtractive coloration scheme, when the absorption resonance is red-shifted, the reflected light has a larger contribution of shorter wavelengths. In contrast, when the resonance is blue-shifted, the reflection is red-shifted. In other words, a red-shift of the absorption curve results in a blue-shift of the color appearance and, conversely, a blue-shift of the absorption results in a hue red-shift. Spectral measurements of the sample at all three temperatures can be seen in Figure 2c. While not much change is observed when changing from 20 to 10 °C, as both temperatures are below LCST, and thus in the hydrophilic phase, at 40 °C the polymer transitions to a hydrophobic state where water is expelled and the polymer layer shrinks, producing a dramatic color change.

We can observe the effect of the humidity in the environment as a driving stimulus for polymer changes by setting the temperature at 20 °C and injecting dynamically nitrogen/water into the atmosphere (Figure 2b). Interestingly, the changes are more marked in the case of humidity variation than temperature variation, even considering that throughout this measurement the

polymer is always under LCST, because in the hydrophilic phase, no phase change occurs. Specifically, when the water content in atmosphere is increased to RH 80%, the polymer absorbs more water molecules as more water is available, producing a subsequent change in thickness that results in a color shift. On the other hand, when the atmosphere is dry, the polymer expels some of the absorbed water and the polymer shrinks. We attribute this behavior to a change in the chemical potential balance between the water in the polymer layer and the atmosphere. As atmosphere is dried, a new balance is found between the polymer and the environment and water is transferred to air to keep it in equilibrium. On the contrary, as the atmosphere becomes more water-saturated, the chemical potential changes sign and, as hydrogen bonds with the monomer chains becomes favored,[44] new water molecules are absorbed by the polymer. Reflection curves for changes in RH with constant temperature can be seen in Figure 2d.

To further assess the optical mechanism, we perform finite difference time domain (FDTD) simulations of the stack at changing polymer thickness (see the Experimental Section). A single aluminum nanoparticle hemisphere with a radius equal to the mean radius of a 5 nm thickness mass equivalent self-assembly is fixed, and the PNIPAM spacer thickness is varied
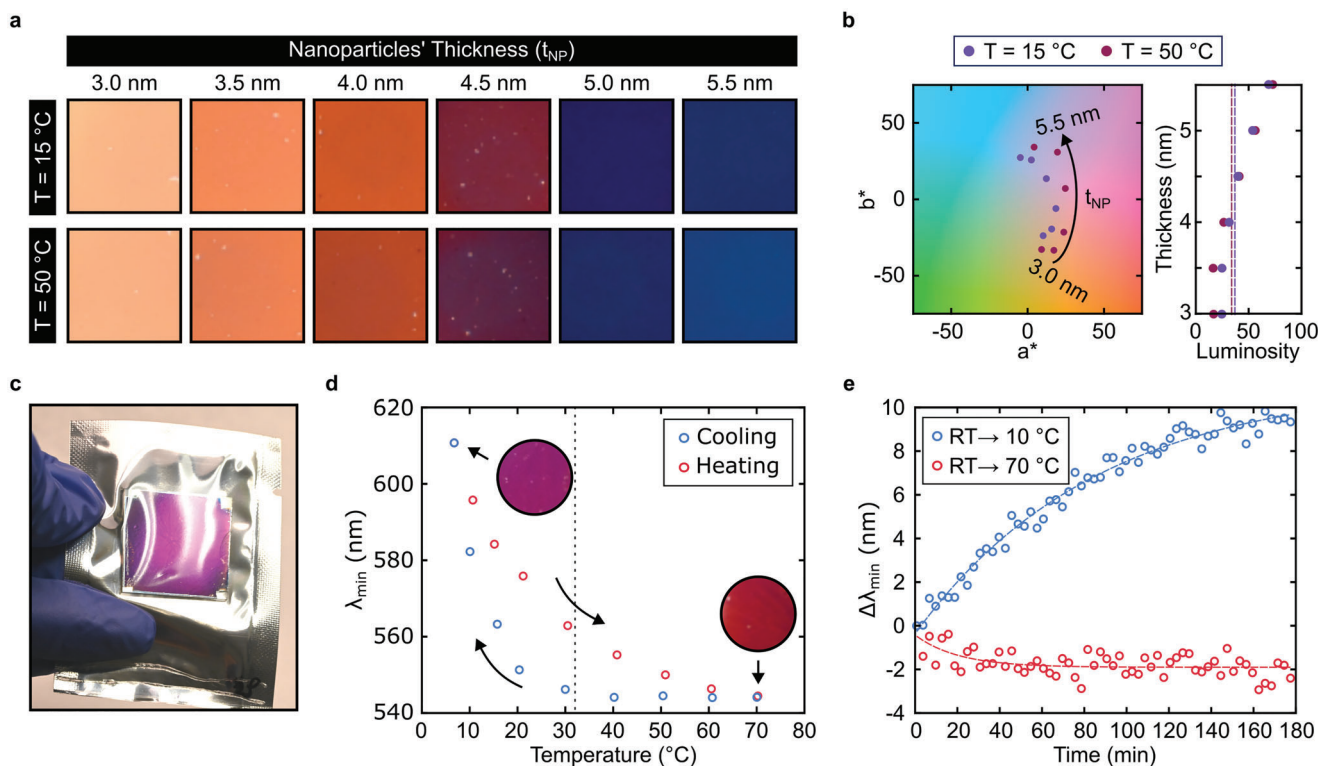
**ADVANCED
SCIENCE NEWS**

www.advancedsciencenews.com

**ADVANCED
OPTICAL
MATERIALS**

www.advopticalmat.de

Figure 3. a) The size of the nanoparticles' layer offers an extra degree of freedom to tailor, at fabrication, the color of the structure. Variation in temperature results in less appreciable color changes for the smaller and larger nanoparticles, whereas is maximum for the central values for which the plasmonic resonance is placed in the center of the visible band. b) CIELAB components of the samples from (a). The arrow shows increasing nanoparticles' layer thickness (t_{NP}) from 3 to 5.5 nm aluminum layer thickness. c) To eliminate the effect of the water content in the atmosphere, the sensors are sealed in an envelope. d) The dynamics of heating and cooling show a clear asymmetry resulting from two different processes, above and below LCST. e) The asymmetry is particularly clear when tracking the spectral shift while heating and cooling a sample from room temperature (20 °C) to 10 and 70 °C.

from 25 to 45 nm. The simulation is performed for a plane wave propagating normal to the stack, and periodic conditions at orthogonal directions. In good agreement with our observation and interpretation, as the thickness of the polymer layer is increased, the reflection minima is shifted to longer wavelengths with no much qualitative change of the resonance shape (Figure 2e–g). To better track the resonance position, we extract the spectral position of the reflection minima every 1 nm of polymer thickness (Figure 2f). The proportionality relation between the thickness of the PNIPAM and the reflection minima position (absorption maxima) clearly shows the behavior previously indicated. Both, lower temperatures and higher humidity favor absorption of water by the polymer and thus swelling, while higher temperatures and drier environments reduce the amount of water in the polymer layer and result in smaller thicknesses. From the slope of Figure 2f, we estimate a spectral shift of 7 nm corresponding to every 1 nm increase of PNIPAM thickness. Interestingly, in contrast to grafted PNIPAM applications where swelling thicknesses can be several times those of the dry polymer, the dynamics of ultrathin films do not show such an extraordinary enlargement. Crucially, this ensures that the polymer thickness remains thin enough to maintain the gap-plasmon hybridization and thus vivid coloration that would be lost in far-field interaction between the self-assembly and the cavity.[46,47]

2.3. Temperature-Responsive Coloration

The color range produced by tuning the structures in response to temperature and humidity changes can also be increased by growing nanoparticle layers of different sizes. Over a PNIPAM layer of 35.5 nm, six different mass thicknesses ranging from 3 to 5.5 nm of aluminum nanoparticles are fabricated. The samples temperature is changed in open atmosphere from 15 °C (below LCST) to 70 °C (above LCST) and photographs are taken (**Figure 3**a). Clearly, the larger particles show a more obvious color change than the smaller ones. As discussed previously, the thickness changes of the polymer spacer tune the resonance by shifting the constructive interference condition of the hybrid gap-plasmon system.[48] For smaller particles however, the plasmonic resonance is found in the violet/near-UV bands, thus small tuning does not affect as much the overall visible color change,[46,47] whereas for bigger particles the plasmon resonance is found in the center of the visible range, where human eye has a better response, and thus can tell colors apart better. Furthermore, as particle size becomes bigger, the plasmon resonance is shifted to the far-red/IR bands, and less obvious change can be appreciated. By measuring the spectra in the hot and cool states and extracting the CIELAB components, the relationship between color change and particle size can be better appreciated (Figure 3b).

**ADVANCED
SCIENCE NEWS**

www.advancedsciencenews.com

**ADVANCED
OPTICAL
MATERIALS**

www.advopticalmat.de

As mentioned before, the maximum appreciable color change is observed for the central bands of the visible wavelengths, where human eyes are more responsive to variations. This corresponds to orange, pink, and purple sensors (nanoparticles sizes corresponding to 4 to 5 nm), whereas for yellow and blue samples (the smallest and biggest nanoparticles' sizes), smaller color change is observed.

To isolate changes in temperature from effects due to changes in humidity, we encapsulate the sensors at RH 50% in a sealed transparent bag, thus fixing the amount of available water, and track the spectral shift of the minimum of the reflection curves with the change in temperature (Figure 3c). Starting at 70 °C, we cool down the sensor to 5 °C and subsequently heat it up again to the initial 70 °C (Figure 3d). Small temperature and time steps are followed (5–10 °C every 15 min) to ensure reaching an equilibrium and avoid device failure as a result of thermal shock. Interestingly, two different regimes seem to be followed when transitioning from a hydrophobic to a hydrophilic phase than the opposite route. In the cooling cycle (blue circles), the shift appears to follow an exponential dependency as water molecules start to be absorbed by the polymer matrix after temperature is dropped below LCST, thus a sharp transition can be indeed seen at above 30–32 °C (dashed line). However, in heating cycle (red circles), two different mechanisms play a role in defining the spectral shift. First, below LCST, temperatures set different balances between water absorbed in the polymer and the environment. However, as the polymer transits to the hydrophobic phase by raising the temperature above LCST, water is expelled and temperature differences only control the kinetics of this desorption process. Indeed, if waited for long enough, the initial spectral position is recovered and the sensor is thus reset (overlapping blue-red circles). Hence, the color shift in response to heating and cooling cycles is observed to be asymmetric, consistent with the asymmetric changes of thickness of ultrathin PNIPAM films reported in literature.[45] This behavior is further confirmed with the next experiment (Figure 3e), where we analyze the time dynamics of a sample as it transiting from room temperature (RT = 20 °C) to 10 °C (blue circles) and from RT to 70 °C (red circles), by placing the samples on a previously cooled/heated stage and track its reflection minima over the course of 180 min. In the case of the cooling experiment, the spectral shift clearly shows the exponential behavior discussed above. Likewise, in the heating experiment, the spectra shift saturates and the shift remains constant as soon as all the water in the PNIPAM is expelled. Considering the larger temperature gradient of this experiment (20 to 70 °C) compared to the one performed in Figure 3d, we can explain the faster character of the shift saturation in this instance.

2.4. Environmental Humidity Colorimetric Sensing

To study with more detail in the effect of the humidity in the color of the sample, we again make use of the custom-made gas chamber (see the Experimental Section). For a sensor at room temperature, nitrogen is injected into the chamber until the RH is dropped to 10%. As explained before, when the atmosphere is dried, the chemical equilibrium is disrupted and water trapped in the polymer tends to evaporate. Consequently, molecules are released reducing the spacer's volume and resulting in an en-

hancement of the red components in the reflected wave (**Figure 4a**). On the contrary, if water vapor is injected into the chamber, the chemical potential is varied and water molecules bond to the polymer chains, producing a swelling of the layer. In this case, more blue components will be present in the reflected light, while red ones will be reduced, pivoting from a pink/magenta appearance to a purple and, finally, blue hue. By injecting water in a control manner, we observe the color change for a 5 nm self-assembly and 35.5 nm PNIPAM film. For eight RHs ranging from 10% to 80%, the samples are photographed registering the subsequent color changes (Figure 4b). Importantly, it should be noted that the temperature is constant and below that of the phase transition in the experiment, thus the color change is the result of changes in thickness in the polymer layer following the desorption of water molecules. Indeed, as the PNIPAM remains in the hydrophilic phase, changes in the atmosphere can be used to tune the thickness smoothly avoiding the characteristic sharp change observed in the case of temperature driven phase transitions. Furthermore, we observe color changes resulting from changes in the water content of the environment to be extremely fast, a matter of a few seconds (see video in Supporting Information). This is a signature of the ultrathin nature of the polymer, where the absorption process is mainly driven by the polymer/air interface, making it a fast sensor. Importantly, the entire process is reversible, and color change is fully recovered when nitrogen or water is injected. Therefore, our hybrid PNIPAM/plasmonic structure works as a reusable, real-time, and powerless humidity sensor. Finally, in contrast to the temperature-driven changes, when humidity is used to drive the color change, no resetting is required on this occasion as shown in Figure 4a.

2.5. Tamper-Resistant Dew Labels

Changes in both temperature and humidity are fully reversible and structures used for the sensing of both stimuli are thus reusable. However, as was noted in the contact angle measurements for temperatures below the LCST (Figure 1c), the presence of a liquid phase on the sensor results in the loss of color and reversibility. This effect presents an interesting opportunity for the production of tamper-resistant condensation labels. Indeed, if the sensor is brought at a temperature below both the LCST and the dew point, then condensation will form and the color will vanish (Figure 4c). The dew point temperature is dependent on both the temperature and the RH of the environment. Therefore, if a sensor is kept at a low temperature in a dry atmosphere, and water vapor at room temperature is slowly injected, after a sufficient amount of water is suspended the dew point condition can be reached and condensation occur. For a sensor at 5 °C and an environment at 20 °C, we find dew forming at an RH close to 40%. Even if the atmosphere is subsequently dried with nitrogen, or the sensor heated to a temperature above LCST, the sensor does not recover the color. It is interesting to notice that this loss of color is not the result of particles being washed away. Instead, when water is condensed on top of the sensor, PNIPAM absorbs water to saturation producing extraordinary swelling of the layer that results in a spacer thickness beyond the one required for the near-field interaction that permits the gap-plasmon modes. Hence, at this extra-large thickness, the plasmons are not
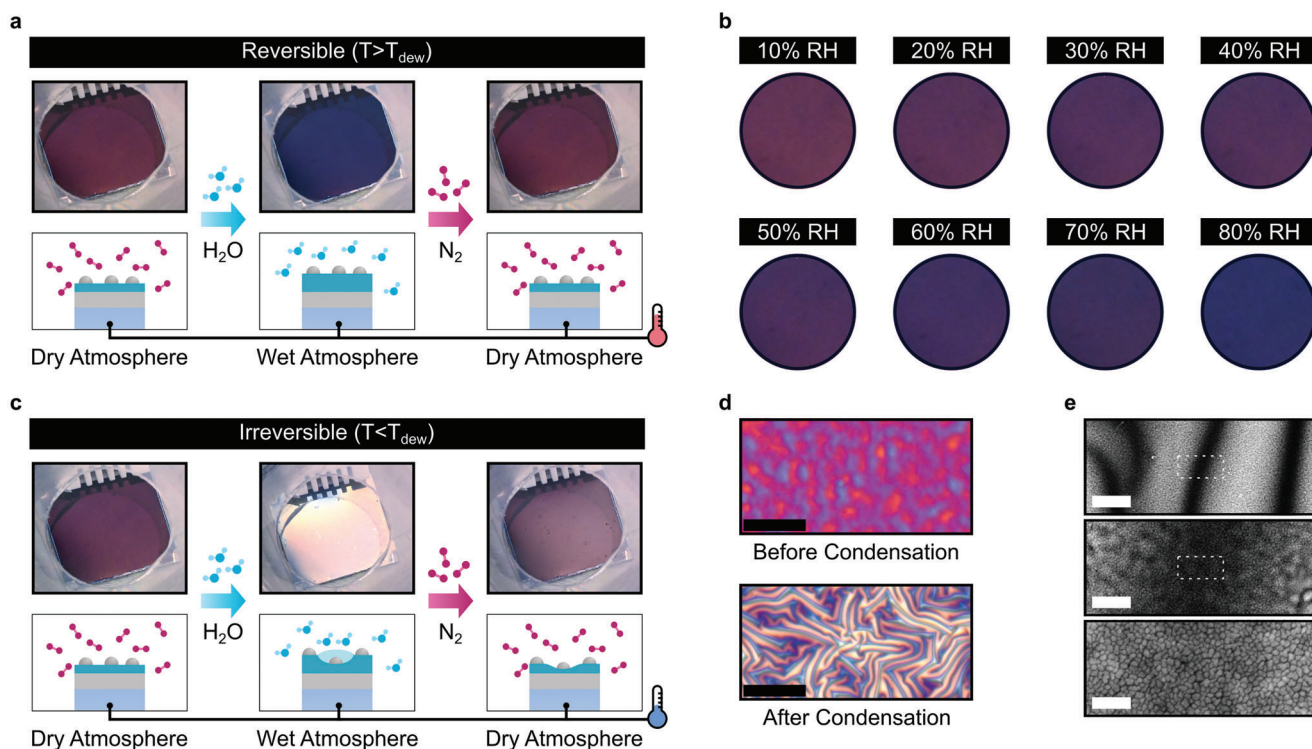
**ADVANCED
SCIENCE NEWS**

www.advancedsciencenews.com

**ADVANCED
OPTICAL
MATERIALS**

www.advopticalmat.de

Figure 4. a) Below the LCST, the structures can be reversibly tuned by changing the humidity in the environment. In a gas chamber, this can be simulated by injecting nitrogen (N_2) or water (H_2O) as needed. b) Changing the humidity in the environment at room temperature (20 °C) from a dry (10% RH) to a wet atmosphere (80% RH), the color can be tuned. c) If water is condensed in the sensor, PNIPAM is oversaturated resulting in an enormous enlargement of the spacer layer that disables the gap-plasmon modes. Even when dried, the color is not recovered. d) Microscope images of the sample before and after condensation (dry states below LCST). e) The peaks and valleys resulting after drying the condensed samples remove irreversibly the color without affecting the nanoparticles. Scale bars for panel (d) are 100 µm. Scale bars for (e), top to bottom, correspond to 10, 2 µm, and 100 nm.

excited anymore and the sensor gets a white appearance corresponding to the back mirror (**Figure 5**c). After drying, the polymer, been deformed beyond recovery, loses the flatness characteristic of the spin-coated samples. Indeed, this drying process creates peaks and valleys of many different heights that produce a washed-color effect that can be understood as the averaging of many different gap-plasmon modes, corresponding to every new thickness of the layer, and resonating at different wavelengths. Optical microscopy and scanning electron microscopy confirm the hypothesis. Microscopic images for a sensor before and after condensation can be found in Figure 4d. Scanning electron microscope (SEM) micrographs of a dried sample (Figure 4e) after condensation shows increased roughness of the film. Although the nanoparticles remain over the entire polymer layer, the PNIPAM now presents a large thickness variability that removes the color. Crucially, even if the atmosphere is subsequently purged, or the sensor heated to a temperature above LCST, the sensor will not recover the color, making it a tamper-proof dew label. Video of the experiment can be found in the Supporting Information.

2.6. Smart Phone-Based Dew Tamper Proofing

To prove the applicability of the sensors for dew label, we developed a simple code that determines the validity of the sensor by analyzing a picture taken with a phone camera in three differ-

ent illuminations (outdoors, and two indoors illuminations). In this manner, a user that, for instance, received a package that was susceptible to condensation would take a picture and the cell phone would determine whether the sensor is valid or tampered (Figure 5a). The code is designed to detect the change in color saturation when condensation occurs (Figure 5b). As was explained before, after condensation and drying the color of the sensor is washed and saturation reduced significantly (Figure 5c). This loss of color saturation can be better appreciated when converting the reflection measurements into hue–saturation–luminosity (HSL) coordinates (Figure 5d). This color space is particularly useful as it reduces the effect of the external illumination in determining the validity of the sensor. Although this effect can be further reduced by using some calibration reference, we find that the use of saturation is a better predictor. The algorithm consists of three simple steps: 1) taking the image, 2) averaging the area of interest to find the color coordinates of the sample, 3) validate the sensor based on saturation levels calculated (see the Experimental Section). A series of four sensors with a droplet shape on a black background are photographed with a smartphone in three illumination contexts (outdoors and two indoors). Two of the sensors correspond to valid samples whereas the other two correspond to dried samples (tamper). The code extracts the color information inside the droplet and calculates the HSL coordinates of the average of the active pixels (those inside the droplet shape). From these triplets, the saturation component proves to be the most
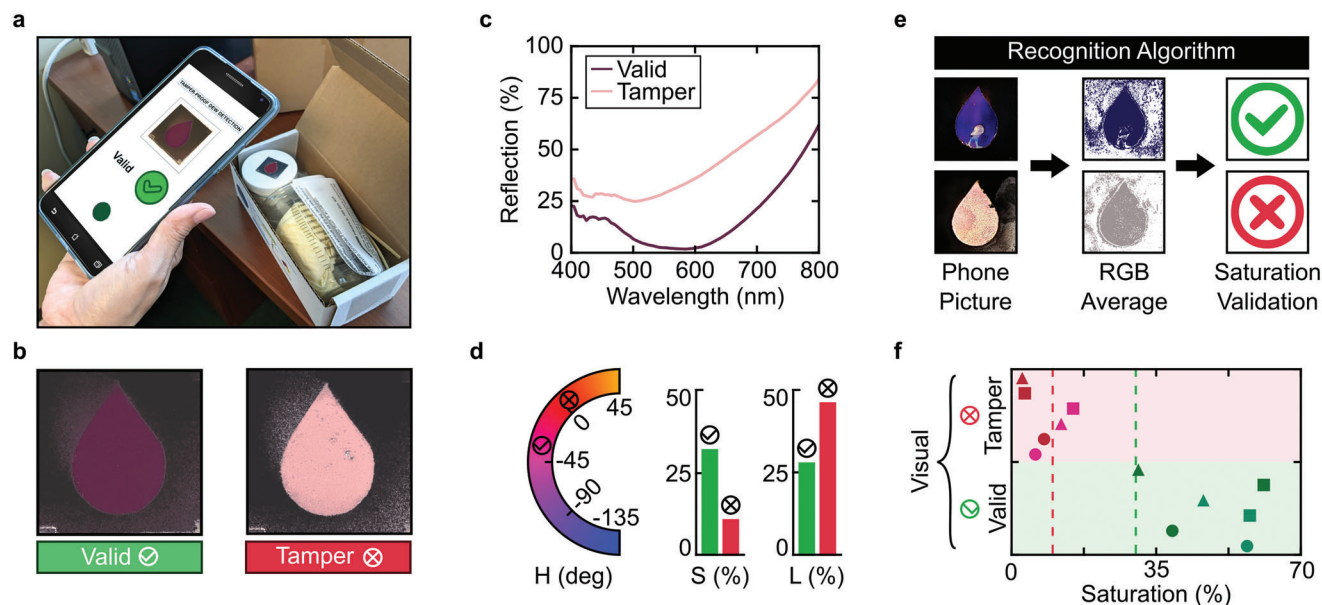
Figure 5. a) A picture captured with a smartphone can be used to determine the validity of a humidity label. b) When a sensor suffers condensation, it will lose its color, not being able to recover it even after drying. To facilitate the detection scheme, a sensor with a droplet shape is used. c) The loss of color saturation is clearly appreciable under spectroscopic analysis. d) Hue (H), saturation (S), and lightness (L) values of the reference values of a valid and tamper labels. e) A simple code extracts from the smartphone picture the relevant pixels, determines their HSL average, and determines their validity based on distance to reference value of saturation. f) While all three HSL values vary according to state (valid and tamper) and illumination context, saturation values are the most robust method of validating the labels. For three different illumination contexts (square, triangle, circle), and three valid (greenish shapes) and three tamper (reddish shapes) samples, saturation values remain clustered around the average of the reference sample (dotted line).

robust method of discrimination. When plotting and comparing to the saturation obtained from spectroscopy measurements of two characteristic sensors (one valid and one tampered, shown in Figure 5c), we observe how the 12 measurements always show to be closer to the spectroscopy-determined saturation regardless of the illumination method (Figure 5f), thus proving the robustness of this simple method.

3. Conclusion

In this work, we have presented a nanosensor based on the hybridization of a temperature and humidity-responsive ultrathin layer of PNIPAM, and a top self-assembly of plasmonic nanoparticles. The stack configuration results in a gap-plasmon mode with strong absorption resonances in the visible that are strongly dependent on the geometry of the structure. Hence, changes in the polymer layer following temperature or changes in the humidity of the environment or the sensor itself result in appreciable color changes that can be used for battery-free reusable temperature and humidity sensors. While many colors can be produced by changing at the design stage the parameters of the nanoparticles layer or the thickness of the spun-coated polymer, we find the pink/purple sensors to show the largest color variability and thus the largest potential in sensing applications. Importantly, actuation with temperature or environmental humidity is totally reversible if no condensation occurs and, after resetting, sensors are ready to be reused again.

Condensation is in many instances an unwanted effect. For instance, in metals results in corrosion and premature fatigue,

while in organic materials favors the growth of mold or bacteria. Unwanted condensation also represents a big problem in storage or shipment that requires controlled climate conditions. Particularly, condensation in cardboard packing material compromises the integrity of the shipment, and for art pieces can be catastrophic.[49,50] We propose that our hybrid PNIPAM/plasmonic color structure can also be used for easy, powerless, and tamper-resistant dew labels, and demonstrate a simple code to determine their validity by taking a smartphone picture. Crucially, benefitted from the fabrication methods employed in the fabrication of the structure, spin coating, and conventional evaporation techniques, the hybrid PNIPAM/plasmonic sensors can be produced in large scale offering a route beyond lab-work for real-world applications.

4. Experimental Section

PNIPAM Ultrathin Film: A clean 1×1 sq. in. microscope slide substrate coated with an optically thick aluminum layer (100 nm) was used as the substrate for the polymer layer. A solution of 200 mg of PNIPAM ($M_n \approx 40\,000$, Sigma-Aldrich) was prepared in 19 g ethanol (200 proof, Sigma-Aldrich) and 1 g of pure water (18.2 MΩ, Thermo Scientific). The water addition was found useful to improve the wettability of the polymer layer to the mirror, Supporting Information Figure S3, ensuring smooth layers. The solution was stirred overnight at RT. The ultrathin films were grown by spin coating 1 mL at 3000 rpm for 30 s to produce 35.5 nm thick films. The samples were then annealed at 70 °C for 3 h (Fisherbrand Isotemp), and stored overnight in a desiccator. After this, samples were ready for the self-assembly growth. Contact angle measurements were performed by dropping 10 µL of water on a thermostage that controlled substrate

**ADVANCED
SCIENCE NEWS**

www.advancedsciencenews.com

**ADVANCED
OPTICAL
MATERIALS**

www.advopticalmat.de

temperature. Videos of the experiment can be seen in the Supporting Information.

Self-Assembled Structural Color Fabrication: An optically thick back-mirror was evaporated by an e-beam evaporator on a clean substrate. After this, the PNIPAM ultrathin film was spin coated. Finally, the self-assembly was grown by e-beam evaporation of aluminum at a very low rate to ensure the Volmer–Weber growth method. Given that the particle sizes were the result of a stochastic growth method, throughout this paper, the self-assembly layer was characterized by the mass thickness equivalent, a parameter controlled during the evaporation. Both, the PNIPAM and self-assembly films for 5 nm, were analyzed in both an atomic force microscopy and SEM systems to analyze their morphology, Supporting Information Figures S1 and S2. For the PNIPAM, an average surface roughness of 2 nm, half of that of the nanoparticles layer, 4.5 nm we found. The variability of the radii of the nanoparticles and the PNIPAM thickness were the two main factors responsible for the broad nature of the absorption resonance (inhomogenous broadening), and the lower spectral purity of the colors.

FDTD Modeling: By analyzing the morphology of the aluminum nanoparticles micrographed by SEM, a histogram of equivalent radii could be extracted, where the equivalent radius of a particle i, r_i^{eq}, is defined as the radius required to fill the area, A_i, of that particle: $r_i^{eq} = \sqrt{A_i/\pi}$, Supporting Information Figure S2b. A Gaussian fit of the histogram permitted the extraction of an equivalent mean radius, while the sum of the areas of the particles over the total area available, A_T, defined the filling factor: $f = (\sum A_i)/A_T$. FDTD (Lumerical Inc.) simulations of a hemispherical particle of mean equivalent radius as extracted from the SEM analysis, with filling factor f, and PNIPAM thicknesses ranging from 25 to 45 nm were run. Square periodic boundary conditions and illumination at normal incidence with a plane wave were set. A monitor was placed on the top of the simulation box to extract the reflection curves. With a MATLAB code, the spectral positions of the minima of the reflection curves as a function of PNIPAM thicknesses obtaining a positive slope of 7 nm red-shift every additional 1 nm of polymer layer, proving the huge sensitivity of the gap-plasmon resonance to the geometrical parameters were tracked. Values for the refractive index of aluminum[51] and PNIPAM[37] were obtained from literature.

Measurements and Images: Reflection curves were taken at normal incidence with unpolarized light using a 4x, 0.07 numerical aperture objective and a fiber-coupled spectrometer (HR 2000+, Ocean Optics). An aluminum mirror was used as a reference to normalize the measurements. To ensure consistency on illumination, the samples were photographed with flash-light at fixed intensity.

Smartphone Validity Check: For the proof of principle, the code to determine the validity of the sensors was built in MATLAB. Nevertheless, this code could be easily integrated on a smartphone application. The code took as input a picture taken from a smartphone. In the first step, it masked the droplet shape from the black background by thresholding and calculated the average RGB values for all the relevant pixels. This average RGB triplet was then converted to HSL according to the following formulas

$$M = \max(R, G, B)$$
$$m = \min(R, G, B)$$
$$C = \text{range}(R, G, B) = M - m \tag{1}$$

where M, m, and C, are, respectively, the maximum, minimum, and chroma components, and the hue (H), saturation (S), and lightness (L), were given by

$$H' = \begin{cases} \text{undefined}, & \text{if } C = 0 \\ \dfrac{G-B}{C} \bmod 6, & \text{if } M = R \\ \dfrac{B-R}{C} + 2, & \text{if } M = G \\ \dfrac{R-G}{C} + 4, & \text{if } M = B \end{cases} \tag{2}$$

$$H = 60° \times H' \tag{3}$$

$$L = \text{mid}(R, G, B) = \frac{1}{2}(M + m) \tag{4}$$

$$S = \begin{cases} 0, & \text{if } L = 1 \text{ or } L = 0 \\ \dfrac{C}{1 - |2L - 1|}, & \text{otherwise} \end{cases} \tag{5}$$

Finally, the saturation value for the picture was compared to two reference values corresponding to one valid and one tamper, whose saturation value was determined from spectroscopic analysis. The sensor was simply ranked as valid or tamper based on the smallest distance to the reference saturations.

Supporting Information

Supporting Information is available from the Wiley Online Library or from the author.

Conflict of Interest

The authors declare no conflict of interest.

Data Availability Statement

The data that support the findings of this study are available from the corresponding author upon reasonable request.

[1] S. Alexander. Maier, *Plasmonics: Fundamentals and Applications*, Springer, New York **2007**.

[2] R. B. Wehrspohn, H.-Siegfried. Kitzerow, K. K. Busch, *Nanophotonic Materials: Photonic Crystals, Plasmonics, and Metamaterials*, Wiley-VCH, Weinheim, Germany **2008**.

[3] B. Deutsch, L. Novotny, P. Bharadwaj, *Adv. Opt. Photonics* **2009**, *1*, 438.

[4] J. A. Schuller, E. S. Barnard, W. Cai, Y. C. Jun, J. S. White, M. L. Brongersma, *Nat. Mater.* **2010**, *9*, 193.

[5] M. E. Stewart, C. R. Anderton, L. B. Thompson, J. Maria, S. K. Gray, J. A. Rogers, R. G. Nuzzo, *Chem. Rev.* **2008**, *108*, 494.

[6] X. Ni, N. K. Emani, A. V. Kildishev, A. Boltasseva, V. M. Shalaev, *Science (1979)* **2012**, *335*, 427.

[7] M. Kang, T. Feng, H.-T. Wang, J. Li, S. Zhang, Y. S. Park, J. Li, X. Lu, W. Zhang, X. Zhang, J. B. Pendry, H. T. Chen, J. Zhou, F. Chen, A. K. Azad, A. J. Taylor, *Opt. Express* **2012**, *20*, 15882.

[8] D. Franklin, Y. Chen, A. Vazquez-Guardado, S. Modak, J. Boroumand, D. Xu, S. T. Wu, D. Chanda, *Nat. Commun.* **2015**, *6*, 7337.

[9] J. Scheuer, *Nanophotonics* **2017**, *6*, 137.

[10] N. Dushkina, A. Lakhtakia, in *Engineered Biomimicry*, (Eds: A. Lakhtakia, R. J. Martín-Palma), Elsevier, New York **2013**, pp. 267–303.

[11] S. Daqiqeh Rezaei, Z. Dong, J. You En Chan, J. Trisno, R. J. H. Ng, Q. Ruan, C. W. Qiu, N. A. Mortensen, J. K. W. Yang, *ACS Photonics* **2021**, *8*, 18.

[12] Z. Xuan, J. Li, Q. Liu, F. Yi, S. Wang, W. Lu, *Innovation* **2021**, *2*, 100081.

[13] Y. Fu, C. A. Tippets, E. U. Donev, R. Lopez, *Wiley Interdiscip. Rev.: Nanomed. Nanobiotechnol.* **2016**, *8*, 758.

[14] J. R. Mejía-Salazar, O. N. Oliveira, *Chem. Rev.* **2018**, *118*, 10617.

[15] N. S. King, L. Liu, X. Yang, B. Cerjan, H. O. Everitt, P. Nordlander, N. J. Halas, *ACS Nano* **2015**, *9*, 10628.

[16] J. R. Fan, J. Zhu, W. G. Wu, Y. Huang, *Small* **2017**, *13*, 1601710.

[17] E. P. A. Van Heeswijk, J. J. H. Kloos, N. Grossiord, A. P. H. J. Schenning, *J. Mater. Chem. A* **2019**, *7*, 6113.

[18] C. Shen, Z. Wang, R. Huang, J. Bao, Z. Li, L. Zhang, R. Lan, H. Yang, *ACS Appl. Mater. Interfaces* **2022**, *14*, 16764.

[19] S. Chervinskii, I. Issah, M. Lahikainen, A. R. Rashed, K. Kuntze, A. Priimagi, H. Caglayan, *ACS Appl. Mater. Interfaces* **2021**, *13*, 50564.

[20] J. Liu, H. Zeng, M. Cheng, Z. Wang, J. Wang, M. Cen, D. Luo, A. Priimagi, Y. J. Liu, *Mater. Horiz.* **2022**, *9*, 942.

[21] H. Meng, J. Hu, *J. Intell. Mater. Syst. Struct.* **2010**, *21*, 859.

[22] S. Wang, Q. Liu, L. Li, M. W. Urban, S. Wang, Q. Liu, L. Li, M. W. Urban, *Macromol. Rapid Commun.* **2021**, *42*, 2100054.

[23] J. Hu, H. Meng, G. Li, S. I. Ibekwe, *Smart Mater. Struct.* **2012**, *21*, 053001.

[24] M. R. Islam, Z. Lu, X. Li, A. K. Sarker, L. Hu, P. Choi, X. Li, N. Hakobyan, M. J. Serpe, *Anal. Chim. Acta* **2013**, *789*, 17.

[25] M. A. Haq, Y. Su, D. Wang, *Mater. Sci. Eng., C* **2017**, *70*, 842.

[26] L. Tang, L. Wang, X. Yang, Y. Feng, Y. Li, W. Feng, *Prog. Mater. Sci.* **2021**, *115*, 100702.

[27] D. Dupin, Z. Deng, Y. Guo, X. Zhao, T. Du, J. Zhu, Y. Xie, F. Wu, Y. Wang, M. Guan, *Gels* **2022**, *8*, 280.

[28] X. Xu, Y. Liu, W. Fu, M. Yao, Z. Ding, J. Xuan, D. Li, S. Wang, Y. Xia, M. Cao, *Polymers* **2020**, *12*, 580.

[29] S. Homaeigohar, M. Elbahri, *Adv. Opt. Mater.* **2019**, *7*, 1801101.

[30] K. Otake, H. Inomata, M. Konno, S. Saito, *Macromolecules* **1990**, *23*, 283.

[31] I. B. Malham, L. Bureau, *Langmuir* **2010**, *26*, 4762.

[32] N. Jiang, X. Zhuo, J. Wang, *Chem. Rev.* **2018**, *118*, 3054.

[33] S. Carregal-Romero, N. J. Buurma, J. Pérez-Juste, L. M. Liz-Marzán, P. Hervés, *Chem. Mater.* **2010**, *22*, 3051.

[34] R. Contreras-Cáceres, J. Pacifico, I. Pastoriza-Santos, J. Pérez-Juste, A. Fernández-Barbero, L. M. Liz-Marzán, *Adv. Funct. Mater.* **2009**, *19*, 3070.

[35] M. Nguyen, X. Sun, E. Lacaze, P. M. Winkler, A. Hohenau, J. R. Krenn, C. Bourdillon, A. Lamouri, J. Grand, G. Lévi, L. Boubekeur-Lecaque, C. Mangeney, N. Félidj, *ACS Photonics* **2015**, *2*, 1199.

[36] M. Toma, U. Jonas, A. Mateescu, W. Knoll, J. Dostalek, *J. Phys. Chem. C* **2013**, *117*, 11705.

[37] H. Gehan, C. Mangeney, J. Aubard, G. Lévi, A. Hohenau, J. R. Krenn, E. Lacaze, N. Félidj, *J. Phys. Chem. Lett.* **2011**, *2*, 926.

[38] L. Yang, X. Fan, J. Zhang, J. Ju, *Polymers* **2020**, *12*, 389.

[39] O. Guselnikova, P. Postnikov, Y. Kalachyova, Z. Kolska, M. Libansky, J. Zima, V. Svorcik, O. Lyutakov, *ChemNanoMat* **2017**, *3*, 135.

[40] W. Wang, E. Metwalli, J. Perlich, K. Troll, C. M. Papadakis, R. Cubitt, P. Müller-Buschbaum, *Macromol. Rapid Commun.* **2009**, *30*, 114.

[41] S. Harms, K. Rätzke, F. Faupel, W. Egger, L. Ravello, A. Laschewsky, W. Wang, P. Müller-Buschbaum, *Macromol. Rapid Commun.* **2010**, *31*, 1364.

[42] W. Wang, G. Kaune, J. Perlich, C. M. Papadakis, A. M. Bivigou Koumba, A. Laschewsky, K. Schlage, R. Röhlsberger, S. v. Roth, R. Cubitt, P. Müller-Buschbaum, *Macromolecules* **2010**, *43*, 2444.

[43] W. Wang, E. Metwalli, J. Perlich, C. M. Papadakis, R. Cubitt, P. Müller-Buschbaum, *Macromolecules* **2009**, *42*, 9041.

[44] Y. Liu, K. Sakurai, *Chem Lett.* **2017**, *46*, 495.

[45] Y. Liu, K. Sakurai, *ACS Omega* **2019**, *4*, 12194.

[46] D. Franklin, Z. He, P. Mastranzo Ortega, A. Safaei, P. Cencillo-Abad, S.-T. Wu, D. Chanda, *Proc. Natl. Acad. Sci. U. S. A.* **2020**, *117*, 13350.

[47] P. Cencillo-Abad, D. Franklin, P. Mastranzo-Ortega, J. Sanchez-Mondragon, D. Chanda, *Sci. Adv.* **2023**, *9*, eadf7207.

[48] M. A. Kats, F. Capasso, *Laser Photonics Rev.* **2016**, *10*, 735.

[49] P. and R. I. of T. Ford, *IPI's Guide to Sustainable Preservation Practices for Managing Storage Environments, Image Permanence Institute*, Rochester Institute Of Technology, Rochester, NY **2012**.

[50] D. V. Chadderton, *Building Services Engineering*, 4th ed., Spon Press, London **2004**.

[51] E. D. Palik, *Handbook of Optical Constants of Solids*, Academic Press, San Diego, CA **1998**.